Journal of Computational Electronics (2018) 17:1640–1649
https://doi.org/10.1007/s10825-018-1243-4

Performance investigation of 120 Gb/s all-optical logic XOR gate using dual-reflective semiconductor optical amplifier-based scheme

Amer Kotb[1,2] · **Kyriakos E. Zoiros**[3] · **Chunlei Guo**[1,4]

Published online: 4 September 2018

Abstract
Reflective semiconductor optical amplifiers (RSOAs) use an anti-reflective coating on the front facet and a high reflectivity coating on the rear facet to produce a higher gain than conventional SOAs. In this paper, this potential is exploited to numerically investigate the ultrafast performance of an all-optical logic XOR gate implemented using a dual-RSOA-based scheme at a data rate of 120 Gb/s. The simulation results demonstrate that the XOR gate is capable of operating at 120 Gb/s with better performance than when using conventional SOAs.

Keywords All-optical XOR gate · Reflective semiconductor optical amplifier · Quality factor

1 Introduction

Modern telecommunication networks are dominated by the unceasing generation, use, and storage of an enormous amount of information. The latter is ubiquitous due to Internet-related services and technological developments such as cloud computing, data centers systems, video on demand, online gaming, and intelligent mobile applications. Employing optical fibers provides a physical medium of huge bandwidth that allows to cope with the continuously increasing traffic of broadband services and satisfy the diverse users' needs. However, the mismatch between fiber-based capacity and operation speed capability of electronic circuitry results in cumbersome optical-to-electrical-to-optical conversions with associated increased cost, power consumption, and complexity. This problematic 'electronic bottleneck' can be overcome by performing several signal processing tasks entirely in the optical domain, i.e., all-optically (AO), and hence directly at the ultra-high speed optical line rate [1]. In particular, the exclusive disjunction (XOR) gate plays a catalytic role in this effort due to its involvement in the execution of numerous signal processing tasks both in fundamental and system-oriented level [2]. The logical operation of this digital gate is such that the outputs are in the 'true' state only when the binary content of both inputs differs.

Given XOR gate significance, various technological approaches, which rely on optical nonlinearities, have been followed for its AO realization [1]. Among them, SOAs, which are active devices having very low reflectivity coatings at both their input and output sides, exhibit the attractive features of strong nonlinearity, compact size, and potential for integration with other optoelectronics devices [3]. For this reason, many demonstrations of all-optical logic XOR gates based on conventional SOAs, either as stand-alone nonlinear elements or incorporated in interferometric configurations, have been reported in the literature [4–12]. However, SOAs also have slow gain and phase recovery times, which limits their signal processing capability to data rates that do not exceed ~ 100 Gb/s and hence cannot follow the upgrades of single-channel data rates into the sub-Tb/s region and beyond [13, 14]. On the other hand, reflective semiconductor optical amplifiers (RSOAs) are a special type of SOAs with an anti-reflective coating on the front facet and a high reflectivity coating on the rear facet, as schematically shown

✉ Amer Kotb
amer@ciomp.ac.cn

Chunlei Guo
guo@optics.rochester.edu

1 The Guo China-US Photonics Laboratory, Changchun Institute of Optics, Fine Mechanics, and Physics, Chinese Academy of Sciences, Changchun 130033, China

2 Department of Physics, Faculty of Science, University of Fayoum, Fayoum 63514, Egypt

3 Lightwave Communications Research Group, Department of Electrical and Computer Engineering, School of Engineering, Democritus University of Thrace, 67100 Xanthi, Greece

4 The Institute of Optics, University of Rochester, Rochester, NY 14627, USA

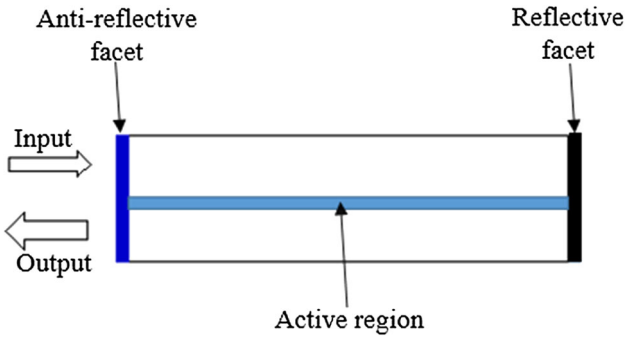

Fig. 1 Schematic of RSOA device

in Fig. 1. Because of this construction, an input signal is amplified and reflected back to the front port, from which it enters the configuration, after passing twice through the active medium. This bidirectional amplification and balanced carrier consumption allow RSOAs to provide higher gain at low injection currents than their ordinary counterparts with a lower noise figure, as well [15]. Owing to these characteristics RSOAs exhibit better modulation behavior than conventional SOAs and have the potential for realizing next-generation broadband access applications [16, 17] and AO switching functionalities [18–20]. In this context, it would further be interesting to investigate whether RSOAs could be exploited for executing the XOR Boolean function exclusively in the optical domain. Unlike previous efforts [18], in this paper, this is done at a data rate of 120 Gb/s, based solely on RSOAs and on cross-phase modulation (XPM) effect in these active devices, which all together constitute a new treatment of the addressed research topic. To this aim, the dependence of the XOR gate quality factor (Q factor) on RSOA and input signal critical operating parameters is examined and assessed by numerical simulations, taking also into account the effect of amplified spontaneous emission (ASE) so as to obtain realistic results. The outcome of this study confirms that the proposed all-optical logic XOR gate using RSOAs can be realized at 120 Gb/s with both logical correctness and high quality. Therefore, the proposed scheme can help XOR gates keep pace with the evolving trends of ultrafast data rates in a feasible and effective manner.

2 RSOAs modeling

The operation of the RSOAs can be theoretically studied based on the computationally efficient and accurate models developed in Refs. [21, 22], which combined with the fundamental formulation in [23] allows to analytically account for interband and intraband nonlinear effects. This is the first time that the specific model is applied in the context of RSOA-based all-optical logic, since until recently this has been done only for RSOA direct amplification [22] or modulation [24]. The model allows calculating the RSOA response to an optical excitation from the solution of a single standard differential equation in the time domain, and hence greatly reduces the computational complexity, while obtaining at least qualitatively meaningful results. This fact strongly differentiates our approach from the simulation method usually followed, which is computationally cumbersome, as it involves solving a set of coupled partial nonlinear differential equations with boundary conditions [25, 26]. By adopting the valid assumptions made therein, the RSOAs time-dependent gains can be derived by numerically solving the following first-order coupled ordinary differential equations:

$$\begin{aligned}\frac{\mathrm{d}h_{\mathrm{CD}}(t)}{\mathrm{d}t} &= \frac{h_0 - h_{\mathrm{CD}}(t)}{\tau_{\mathrm{c}}} \\ &- \frac{h_{\mathrm{CD}}(t)}{h_{\mathrm{CD}}(t)} - \alpha_{\mathrm{loss}}L(\exp[h_{\mathrm{CD}}(t) + h_{\mathrm{CH}}(t) \\ &+ h_{\mathrm{SHB}}(t) - \alpha_{\mathrm{loss}}L] - 1) \times (1 + R\exp[h_{\mathrm{CD}}(t) + h_{\mathrm{CH}}(t) \\ &+ h_{\mathrm{SHB}}(t) - \alpha_{\mathrm{loss}}L])\frac{P_{\mathrm{in}}(t)}{E_{\mathrm{sat}}} \end{aligned} \quad (1)$$

$$\begin{aligned}\frac{\mathrm{d}h_{\mathrm{CH}}(t)}{\mathrm{d}t} &= -\frac{h_{\mathrm{CH}}(t)}{\tau_{\mathrm{CH}}} \\ &- \frac{\varepsilon_{\mathrm{CH}}}{\tau_{\mathrm{CH}}}(\exp[h_{\mathrm{CD}}(t) + h_{\mathrm{CH}}(t) + h_{\mathrm{SHB}}(t) - \alpha_{\mathrm{loss}}L] - 1) \\ &\times (1 + R\exp[h_{\mathrm{CD}}(t) + h_{\mathrm{CH}}(t) + h_{\mathrm{SHB}}(t) - \alpha_{\mathrm{loss}}L])P_{\mathrm{in}}(t) \end{aligned} \quad (2)$$

$$\begin{aligned}\frac{\mathrm{d}h_{\mathrm{SHB}}(t)}{\mathrm{d}t} &= -\frac{h_{\mathrm{SHB}}(t)}{\tau_{\mathrm{SHB}}} \\ &- \frac{\varepsilon_{\mathrm{SHB}}}{\tau_{\mathrm{SHB}}}(\exp[h_{\mathrm{CD}}(t) + h_{\mathrm{CH}}(t) + h_{\mathrm{SHB}}(t) - \alpha_{\mathrm{loss}}L] - 1) \\ &\times (1 + R\exp[h_{\mathrm{CD}}(t) + h_{\mathrm{CH}}(t) + h_{\mathrm{SHB}}(t) \\ &- \alpha_{\mathrm{loss}}L])P_{\mathrm{in}}(t) - \frac{\mathrm{d}h_{\mathrm{CD}}(t)}{\mathrm{d}t} - \frac{\mathrm{d}h_{\mathrm{CH}}(t)}{\mathrm{d}t} \end{aligned} \quad (3)$$

where functions 'h' represent the RSOAs' gain, which is integrated over the RSOAs' length and is induced during the dynamic processes of carrier depletion (CD), carrier heating (CH), and spectral hole burning (SHB). $G_0 = \exp[2h_0]$ [22], where G_0 is the unsaturated power gain and the multiplicative factor of two in front of h_0 takes into account the double pass of the signal inside the RSOAs active region of rear-facet reflectivity (R), internal loss coefficient (α_{loss}), and length of active region (L). $E_{\mathrm{sat}} = P_{\mathrm{sat}}\tau_{\mathrm{c}}$ is the RSOAs saturation energy, where P_{sat} is the saturation power and τ_{c} is the carrier lifetime. $P_{\mathrm{in}}(t)$ is the time-dependent power of the data inserted in the RSOAs, which is linked to light intensity, $S(t)$, through $P(t) = \kappa\ S(t)$, where κ denotes the conversion factor from the photon density of power. τ_{CH} and τ_{SHB} are the temperature relaxation rate and the carrier–carrier scattering rate, respectively. $\varepsilon_{\mathrm{CH}}$ and $\varepsilon_{\mathrm{SHB}}$ are the nonlinear gain suppression factors due to CH and SHB, respectively.

The total gain $G(t)$ of each RSOA is then given by [21]:

$$G(t) = R\ \exp[2(h_{\mathrm{CD}}(t) + h_{\mathrm{CH}}(t) + h_{\mathrm{SHB}}(t) - \alpha_{\mathrm{loss}}L)] \quad (4)$$

While the associated phase change incurred on a signal propagating through the RSOAs as a result of their gain perturbation is given by:

$$\Phi(t) = -(\alpha\, h_{\mathrm{CD}}(t) + \alpha_{\mathrm{CH}}\, h_{\mathrm{CH}}(t) + \alpha_{\mathrm{SHB}}\, h_{\mathrm{SHB}}(t)) \quad (5)$$

where α is the traditional linewidth enhancement factor (α factor) associated with interband carrier dynamics, α_{CH} is the linewidth enhancement factor due to CH and α_{SHB} is the linewidth enhancement factor due to SHB. The contribution governed by α_{SHB} is null because SHB produces a nearly symmetrical spectral hole centered at the signal wavelength. In this case, the Kramers–Kronig integral becomes antisymmetric at the operating frequency and the Kramers–Kronig integral remains very small [27].

In the simulation, the input data streams are assumed to be Gaussian-shaped with a FWHM (full width at half maximum) pulse width (τ_{FWHM}) and default value of 1/8 the bit period (T = 8.33 ps @ 120 Gb/s), which is the inverse of the data repetition rate. The input power profile is described by [3, 4]:

$$\begin{aligned} P_{A,\,B}(t) &\equiv P_{\mathrm{in}}(t) \\ &= \sum_{n=-\infty}^{n=+\infty} a_{nA,B}\, \frac{2\sqrt{\ln(2)}\, E_0}{\sqrt{\pi}\ \tau_{\mathrm{FWHM}}} \exp\left[-\frac{4\ln(2)(t - n\,T)^2}{\tau_{\mathrm{FWHM}}^2}\right] \end{aligned} \quad (6)$$

where $a_{nA,B}$ is the n-th pulse, which can take the logical value '1' or '0' and E_0 is the pulse energy. n is the length of the pseudorandom binary sequence (PRBS), which is $2^7 - 1$ bits-long.

It should be noted that the applied RSOA model is not compromised by the RSOA round-trip structure nor by the picosecond scale of the propagating signals which are factors that combined would prevent the accurate description of the RSOA dynamics. In fact, the key for switching is exploiting and perturbing the maximum possible gain that the RSOA can offer, which occurs at the middle of its active region (cf. Fig. 5 in [21]). Consequently, the time that must elapse for the first pulse that enters the RSOA to be reflected back and encounter the peak of the available gain is $T_{\mathrm{transit}} + T_{\mathrm{transit}}/2 = 6$ ps, where $T_{\mathrm{transit}} = 4$ ps is the single-pass transit time that corresponds to the 0.4 mm-long RSOA cavity used in the simulations. In this case, the forthcoming pulse heading in the forward direction from the RSOA front facet to the RSOA center will not have reached and traveled past this point but will need 4.3 ps more since it physically lags behind by $T_{\mathrm{per}} + T_{\mathrm{transit}}/2$. In this manner, the RSOA gain dynamics will be distinctly modified without being affected by pulse round-trip (RT) delay, even if the latter is higher than the pulses' FWHM. This is an important difference against [22], which concerns direct amplification, and not switching, of a single pulsed signal. Thus the physical mechanism of operation differs in that the RSOA gain change is induced and perceived by the inserted signal itself and is not mapped on a second, coexisting signal, such as a CW input beam. In this case, it will take a total of 9 ps for a 1 ps-width pulse to alter the RSOA gain and be amplified at its exit after having traveled the RT interval of 8 ps. This means that the whole amplification process will not have been completed when the next pulse arrives after ~ 8.3 ps, and hence will be impaired, thus necessitating to invoke the reduced RSOA model criterion [22].

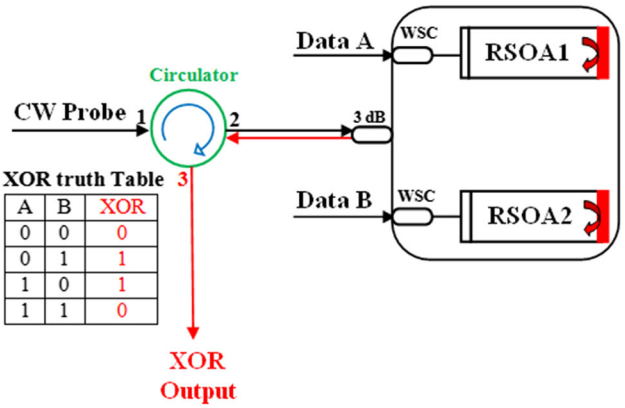

Fig. 2 Schematic diagram and truth table of dual-RSOA-based XOR gate. A circulator is employed to insert and extract the continuous wave (CW) beam on which the outcome of all-optical XOR operation is mapped. *WSC* wavelength selective coupler

3 All-optical XOR gate with dual-RSOA-based scheme

3.1 Operation principle

Figure 2 shows the schematic diagram and the truth table of the dual-RSOA-based XOR gate. For XOR operation, two modulated data signals A and B are inserted in two respective RSOAs, RSOA1 and RSOA2. In parallel, a continuous wave (CW) beam is split by a 3 dB coupler into a pair of identical parts, which drive the RSOAs concurrently with their data signals counterparts. Two reciprocal wavelength selective couplers (WSCs) are used to combine the CW input with data signals A and B launched into RSOA1 and RSOA2, respectively, in the forward direction, and split the composite output from the RSOAs in the backward direction to extract the CW signal that carries the logical result of XOR operation and isolate the perturbing signals A and B. Typical

values for the losses and bandwidth of these components when handling signals located in optical communications C-band spectral region are 0.7 dB and 40 nm, respectively, as it can be found from various photonic manufacturers' product catalogues. Compared to the input signals' peak power these losses are extremely low and are not capable of altering the RSOAs specified degree of saturation. Therefore, they can be ignored without affecting the essence of the results obtained from the conducted theoretical treatment.

3.2 Simulation

The output power of the XOR gate is described by the following equation:

$$P_{\mathrm{XOR}}(t) = 0.25\, P_{\mathrm{CW}}(G_1(t) + G_2(t) - 2\sqrt{G_1(t)\, G_2(t)}\cos\left[\Phi_1(t) - \Phi_2(t)\right]) \quad (7)$$

where P_{cw} stands for the CW beam power, while $G_{1,2}(t)$ and $\Phi_{1,2}(t)$ are the time-dependent total gains and phase shifts experienced by the copies of the CW beam inside RSOA1 and RSOA2, respectively. This output is critically affected by a set of key operating parameters, which include the RSOAs' device building, structural, driving, and input signal characteristics. Thus, in order to improve the performance of the proposed XOR gate at the target data rate, these parameters should be optimized. This can be done through numerical simulation, which has been prepared and run in Wolfram Mathematica®. For fair performance comparison between RSOAs and SOAs, the same parameters values listed in Table 1 have been employed for both devices, which are simulated using the same model formulation, except that for the SOA the reflectivity, R, is set to zero and the unsaturated power gain is $G_0 = \exp[h_0]$, as opposed to $R = 1$ and $G_0 = \exp[2h_0]$ for the RSOA.

The metric against which the performance of the XOR gate is investigated and evaluated is the Q factor, which is defined as $Q = (P_1 - P_0)/(\sigma_1 + \sigma_2)$ [3, 4], where $P_{1,0}$ are the average powers of the '1's and '0's expected at the output and $\sigma_{1,2}$ are the corresponding standard deviations. For acceptable performance, the Q factor must be over six to ensure a bit error rate of less than 10^{-9} [3]. By designing the XOR gate as deduced from the interpretation of the Q factor versus critical parameters curves shown in the following paragraphs, the Q factor value is found to be 35 at 120 Gb/s, which is higher than that reported on all-optical XOR gate works with conventional SOAs [3–12]. Figure 3, which shows the simulation results for the XOR operation between indicative patterns of data signals A and B at 120 Gb/s, also confirms that the specific Boolean logic is executed both with logical correctness and high quality with regard to the outcome pulses profile and eye diagram.

Table 1 Simulation parameters

Symbol	Definition	Value	Unit
E_0	Pulse energy	0.22	pJ
τ_{FWHM}	Pulse width	1	ps
n	PRBS length	127	–
T	Bit period	8.33	ps
λ_{A}	Wavelength of signal A	1555	nm
λ_{B}	Wavelength of signal B	1555	nm
λ_{CW}	Wavelength of CW beam	1557	nm
P_{CW}	Power of CW beam	0.08	mW
T_{op}	Operating temperature	290	K
I	Injection current	100	mA
P_{sat}	Saturation power	10	mW
R	Rear-facet reflectivity	1	–
L	Length of active region	0.4	mm
d	Thickness of active region	0.3	μm
α_{loss}	Internal loss coefficient	10	mm^{-1}
Γ	Confinement factor	0.15	–
τ_{c}	Carrier lifetime	100	ps
α	Traditional linewidth enhancement factor	4	–
α_{CH}	Linewidth enhancement factor due to CH	1	–
α_{SHB}	Linewidth enhancement factor due to SHB	0	–
τ_{CH}	Temperature relaxation rate	0.3	ps
τ_{SHB}	Carrier-carrier scattering rate	0.1	ps
$\varepsilon_{\mathrm{CH}}$	Nonlinear gain suppression factor due to CH	0.02	W^{-1}
$\varepsilon_{\mathrm{SHB}}$	Nonlinear gain suppression factor due to SHB	0.02	W^{-1}
G_0	Unsaturated power gain	15	dB
N_{sp}	Spontaneous emission factor	2	–

On the other hand, the output signal (XOR) is not fully extinguished at the bit slots where both data are present, i.e., 'A' = 'B' = '1,' and where a logical '0' is expected. Nevertheless, the peak amplitude difference between '1's and '0's is over 10 dB, which guarantees the unambiguous discrimination between them [2]. This is also reflected on the eye diagram, since the border of the low binary level is not perfectly thin but exhibits an analogous vertical deviation from the perfect '0' ground.

Figure 4 shows the Q factor dependence on the RSOAs rear-facet reflectivity for the XOR operation at 120 Gb/s.

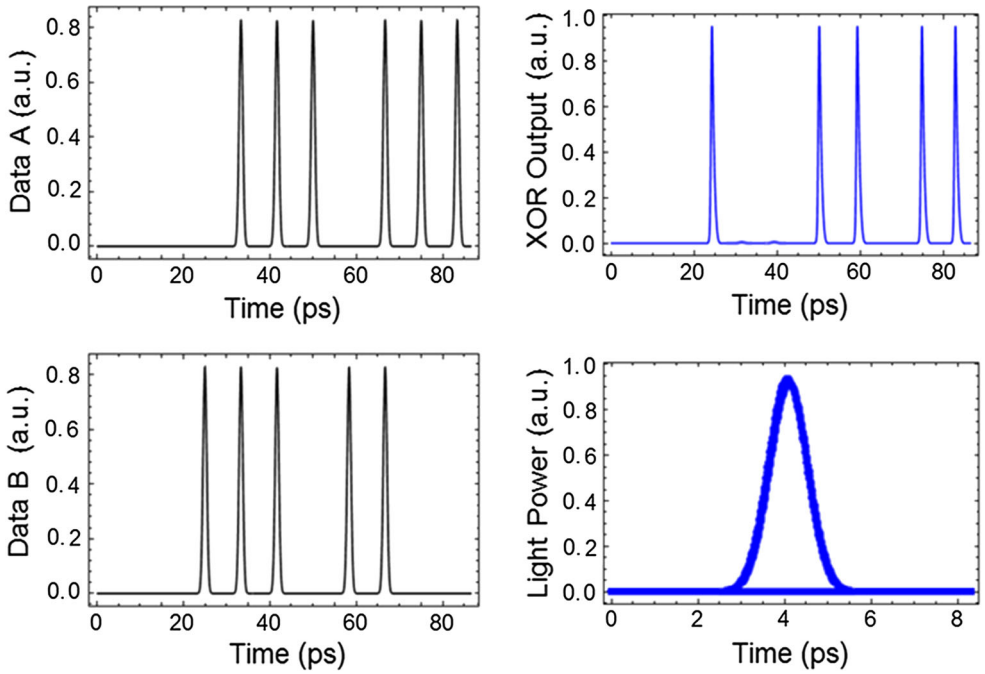

Fig. 3 Simulation results of dual-RSOA-based XOR operation at 120 Gb/s. The achieved Q factor is 35

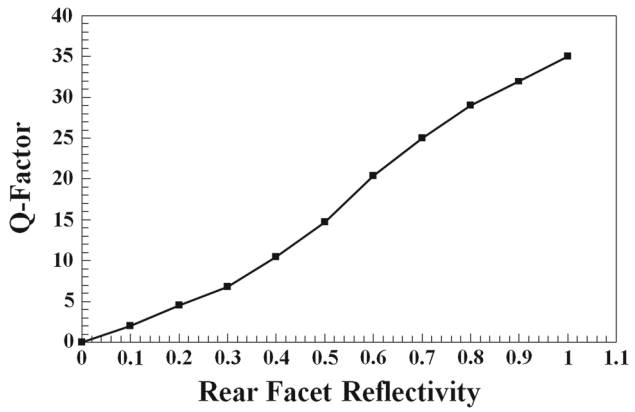

Fig. 4 Q factor versus RSOAs rear-facet reflectivity

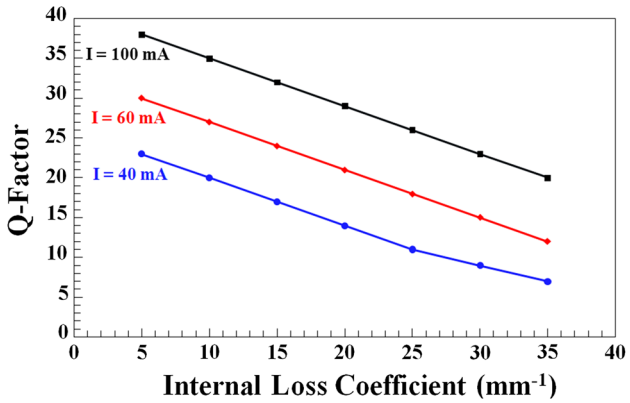

Fig. 5 Q factor versus RSOAs internal loss coefficient

From this figure, it is clearly seen that the Q factor is rather increased as the rear-facet reflectivity becomes higher. This happens because the propagating input signal is amplified and reflected back more efficiently by the rear facet to the point that when it reaches the front port it receives twice as much gain as in usual SOAs. This makes a significant difference concerning the design and the construction of the proposed employed active devices over their conventional counterparts.

Insight into the performance of the dual-RSOA-based XOR gate can be acquired by monitoring in Fig. 5, which shows the Q factor as a function of the internal loss coefficient for different values of operating currents. From this figure, it can be seen that although the Q factor is decreased as internal losses become more pronounced, nevertheless their impact can be mitigated by raising the injection current at the expense of increased power consumption. Thus, an injection current of 100 mA must be supplied to RSOAs to compensate for internal losses of 10 mm^{-1} and obtain a Q factor of 35.

The Q factor's dependence on the length and thickness of the RSOA and the standard SOA is shown in Fig. 6a, b, respectively. These figures have been obtained by keeping the current density constant [28] to 83 kA/cm^2 and properly adjusting the confinement factor so that the ratio of this parameter to the active region cross-sectional area, and accordingly the saturation energy, is kept fixed [29]. From this figure, it can be seen that the Q factor is increased for a longer RSOA and this improvement is more significant than

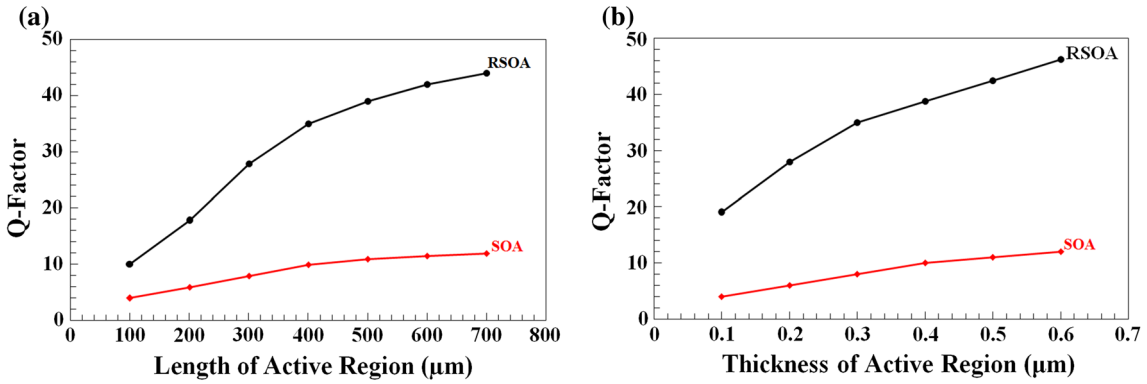

Fig. 6 Q factor versus active region **a** length and **b** thickness for RSOA- and standard SOA-based XOR operation

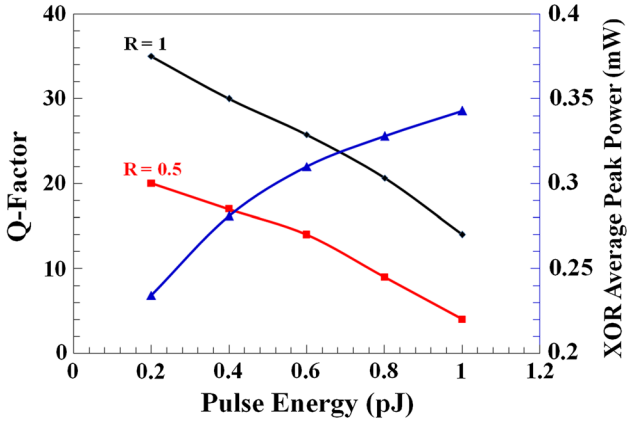

Fig. 7 Q factor and XOR average peak power versus RSOAs input pulse energy

for the same length of conventional SOA. This difference is attributed to the RSOA double-pass configuration, which allows enough space to induce more strongly the nonlinear differential phase shift and make the latter accumulate closer to the level of optimum switching. Moreover, the highest Q factor achieved with the longest SOA is almost the same with the lowest value of this metric achieved with the shortest RSOA. Similar observations qualitatively hold with regard to the thickness of the active region of these devices. Therefore, it can be deduced that the XOR gate can be realized with an acceptable performance by means of RSOAs whose total size is more compact than that of conventional SOAs.

The Q factor dependence on the pulse energy for different values of RSOAs rear-facet reflectivity is shown in Fig. 7. As pulses become more energetic, the Q factor is reduced due to the heavier RSOA gain saturation. In order to keep the Q factor acceptable, the RSOA must be full and not half-reflective so as to take full advantage of the feedback process inside the RSOA cavity and maximize the perturbation of the concomitantly offered gain. The highest possible reflectivity also results in a better Q factor for the same pulse energy. A Q factor of 35 is obtained for a pulse energy of 0.22 pJ, which is of the order of that used in SOA-based AO gates operating at sub-Tb/s rates [30] and corresponds to an average peak input data power of ~ 5.4 dBm, which also is considered a rational amount for AO switching purposes. The secondary 'y'-axis displays the average peak power of the XOR output sequence as a function of the input pulse energy. From these extra values, it can be deduced that the RSOAs gain perturbation from the unsaturated level lies in the vicinity of deep saturation [31].

Figure 8 shows the Q factor dependence on the RSOAs operating temperature. From this figure, it can be seen that the Q factor is higher at lower temperatures for different values of moderate injection current. Physically, this occurs because the distribution of free carriers and the nonradiative recombination become such that favor the supply of more gain [32], which in turn causes the Q factor to increase. First, the probability of carriers to occupy the active medium energy levels increases with a decrease in temperature. Second, electrons are distributed over a narrow range at a lower temperature and hence the number of these carries available for participating in optical transition, thus providing gain, at a given energy becomes more. Third, nonradioactive recombinations, which decrease with a decrease in the device temperature, cause an increase in the gain for a given current. Moreover, the temperature decrease accelerates the gain recovery of RSOAs [32], which hence become more capable of handling ultrafast data so that the latter can undergo the XOR operation with better performance. Therefore, RSOAs employed for ultrafast switching in an all-optical interferometric-based gate should be operated at low temperature. This condition can be satisfied by placing the RSOAs chips in TO-can packages [33], which is a possible way for ensuring efficient cooling during operation.

The dependence of Q factor on the pulse width and carrier lifetime for the RSOA and the standard SOA is shown in Fig. 9a, b, respectively. More specifically, Fig. 9a, which has been obtained for constant pulse energy according to Table 1, shows that the Q factor decreases as pulses become

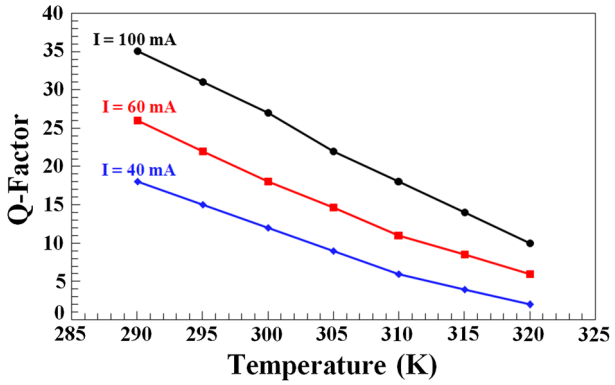

Fig. 8 Q factor versus RSOAs temperature for different injection currents

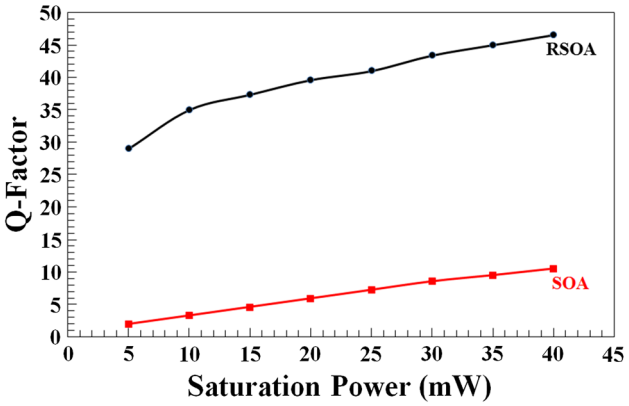

Fig. 10 Q factor versus saturation power for RSOA- and conventional SOA-based XOR operation

broader. This happens because in this case the pulse peak power, which scales inversely with the examined parameter [34], changes into the opposite direction so that the RSOAs become less saturated than they should for proper execution of the XOR operation. This implies that employing RSOAs instead of SOAs can relax the requirements on the optical sources and optical time division multiplexing needed to generate these pulses and allocate them to bit slots, respectively [13]. A similar trend is observed for the variation of the Q factor against the carrier lifetime, which suggests that preferring the RSOA over the SOA can help avoid resorting to sophisticated gain recovery acceleration techniques.

The Q factor dependence on the saturation power is shown in Fig. 10 for the RSOA and the conventional SOA-based XOR operation. It is seen that although the Q factor rises in both cases, yet it becomes acceptable across the whole scanned range of the saturation power only for the RSOA. This allows to have more freedom in the design of the RSOA and achieve switching in a more power-efficient manner. For the conventional SOA, on the other hand, a comparatively higher saturation power is required to render the Q factor acceptable. Inversely, for a saturation power of 10 mW, for which the Q factor is 35 when RSOAs are employed, it is not possible to attain the same value for the SOA case, since this metric is more than seven times lower as well as unacceptable. The physical explanation for this difference lies in the different construction and operation of the two types of SOAs. Thus, a conventional SOA is a single-pass amplifier whose gain saturates monotonically with the optical power increase along the length of the device. In the RSOA, in contrast, a fraction of incident light is reflected at the rear facet and travels back through the active medium. As a consequence, the forward and backward traveling waves compete to gain from the same source of carriers, which results in stronger gain saturation [15]. The reason that performance-degrading pattern effects do not manifest in the RSOA-based XOR gate, thus enabling to achieve high Q factor values, is because the RSOAs are driven into strong saturation subject to which they exhibit an effective carrier lifetime that is smaller than the pulses' repetition period. In fact, the calculated [35] value of the former parameter is nearly half that of the latter, which allows supporting ultra-high data rate all-optical Boolean logic with pattern-free performance. This ultrafast signal handling capability is concurrently enhanced for RSOAs high rear-facet reflectivi-

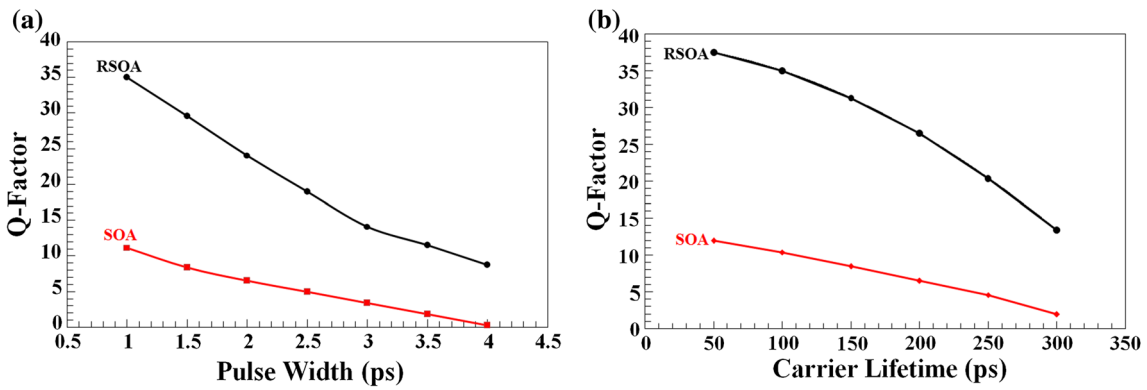

Fig. 9 Q factor versus **a** input pulse width and **b** carrier lifetime for RSOA- and SOA-based XOR operation

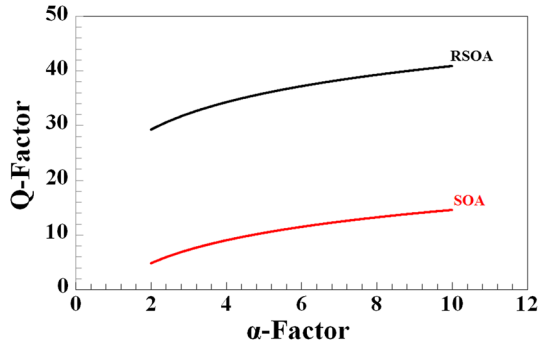

Fig. 11 Q factor versus traditional linewidth enhancement factor (α factor) for RSOA- and conventional SOA-based XOR operation

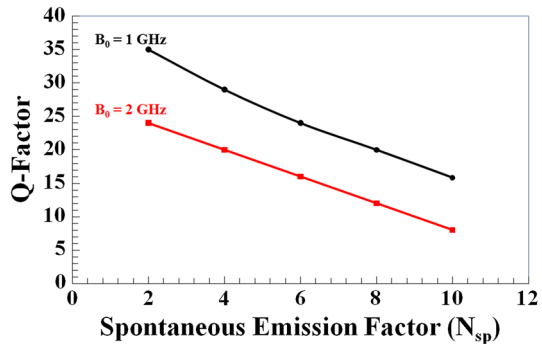

Fig. 12 Q factor versus RSOAs spontaneous emission factor (N_{sp}) for different optical bandwidths

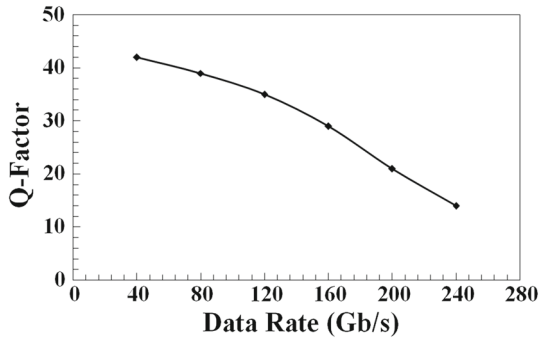

Fig. 13 Q factor versus data rate for RSOA-based XOR operation

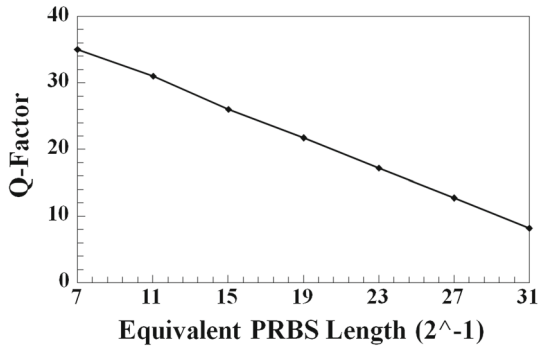

Fig. 14 Q factor versus equivalent PRBS length

ties [36]. Thus, performance-degrading pattern effects do not manifest in the considered RSOA-based XOR gate scheme, as verified by observing Fig. 3, thus enabling to achieve high Q factor values.

The simulated Q factor versus the α factor for the RSOA and the conventional SOA-based XOR operation is shown in Fig. 11. The Q factor increases as the α factor is increased because in this case the induced phase changes are intensified and affect analogously the magnitude of the marks produced from the XOR function. Furthermore, when RSOAs are used, the Q factor is higher and acceptable, even for small α factor values, while this is not possible with the standard SOAs. Since the values of this parameter change depending on the operating conditions [27], this means that its adjustment can be less demanding, which is clearly desirable from a practical perspective.

The amplified spontaneous emission (ASE) acts as noise on optical amplifiers, thus causing the degradation of their performance and subsequently of the circuits in which they are embedded. In this simulation, we took into account the impact ASE on the Q factor. This is done through the ASE's noise related to the spontaneous emission factor (N_{sp}), which is expressed by the following equation [3]:

$$P_{ASE} = N_{sp}(G_0 - 1)\, K\, \upsilon B_0 \tag{8}$$

where N_{sp} is the spontaneous emission factor, K is Planck's constant, and B_0 is the optical bandwidth at an optical frequency (υ). Equation (8) is universal regardless of the specific optical amplifier type [37], which in turn is accounted for by replacing the corresponding gain factor mentioned in Table 1. Using it in our case implies that ASE noise does not affect the RSOA gain dynamics [38]. This assumption is valid since the RSOAs are operated around deep saturation where the optical gain is not affected by ASE. The ASE noise calculated from Eq. (8) is numerically added to the power of the XOR output pulses given from Eq. (7) [38]. The Q factor variation versus N_{sp} for the RSOA is shown in Fig. 12 for different optical bandwidths. It can be seen that even when the contribution of ASE is aggravated, the performance of the scheme remains acceptable, preferably when having a narrower optical bandwidth which helps reject more strongly the out-of-band noise.

The Q factor versus the data rate for the RSOA-based XOR operation is shown in Fig. 13. The horizontal axis values scanned for this purpose have an upper limit of 250 Gb/s, which is set by the requirement that the pulse repetition period must exceed the RSOAs one-way propagation time, as explained at the end of Sect. 2. Then, all-optical Boolean functionalities, like those considered in this paper, can be achieved at data rates, B, as fast as inversely proportional to RSOAs transit time, i.e., $B \leq (1/T_{transit}) =$ (1/4) * 1000 Gb/s = 250 Gb/s. Although the Q factor is

decreased with the increase in the data rate, yet it remains high and acceptable when using RSOAs.

Figure 14 shows that the operation of the XOR gate is affected by higher equivalent lengths [39] of the PRBS carried by each input data. The horizontal axis represents the number of consecutive '0's and '1's contained in each data sequence driving the RSOAs and agrees with PRBS's 'balance' property, which states that if the PRBS order is 'n' then it contains '$n-1$' consecutive zeros and 'n' consecutive ones [40]. This approach is more computationally affordable than if the full PRBS length, which scales with the power of '2,' i.e., 2^n-1, were used, but still, the 'equivalent' PRBS to which these strings correspond can sufficiently stress the XOR gate operation. Despite the increased strain imposed by longer PRBS, the scheme is tolerant to this effect and retains its acceptable performance.

4 Conclusions

In conclusion, the possibility of designing an all-optical logic XOR gate by using a scheme based on dual-reflective semiconductor optical amplifiers as nonlinear elements has been investigated and demonstrated through numerical simulation and theoretical analysis. The specific Boolean function can be executed both with logical correctness and high quality between data of 120 Gb/s repetition rate, as indicated by the more than acceptable performance metric achieved for a technologically rational and feasible selection and the combination of the critical operating parameters. Moreover, the obtained results suggest that the ultrafast performance of the XOR gate based on RSOAs is better and less technologically challenging than if conventional SOAs were used instead. Although there certainly are margins for further improvements with regard to modeling and results accuracy, we believe that this does not compromise the main conclusions drawn from the presented work, which can actually spur the design and construction of complex circuits and subsystems of enhanced logic functionality that rely on the RSOA-based XOR gate.

Acknowledgments The authors would like to thank the editor of the journal and anonymous reviewers.

References

1. Willner, A.E., Khaleghi, S., Chitgarha, M.R., Yilmaz, O.F.: All-optical signal processing. J. Lightwave Technol. **32**, 660–680 (2014)
2. Dimitriadou, E., Zoiros, K.E.: All-optical XOR gate using single quantum-dot SOA and optical filter. J. Lightwave Technol. **31**, 813–3821 (2013)
3. Dutta, N.K., Wang, Q.: Semiconductor Optical Amplifiers, 2nd edn. World Scientific Publishing Company, Singapore (2013)
4. Kotb, A.: All-Optical Logic Gates Using Semiconductor Optical Amplifier. Lambert Academic Publishing, Saarbrucken (2012)
5. Chen, H., Zhu, G., Wang, Q., Jaques, J., Leuthold, J., Piccirilli, A.B., Dutta, N.K.: All-optical logic XOR using a differential scheme and Mach–Zehnder interferometer. Electron. Lett. **38**, 1271–1276 (2002)
6. Wang, Q., Zhu, G., Chen, H., Jaques, J., Leuthold, J., Piccirilli, A.B., Dutta, N.K.: Study of all-optical XOR using Mach–Zehnder interferometer and differential scheme. IEEE J. Quantum Electron. **40**, 703–709 (2004)
7. Kim, J.Y., Kang, J.M., Kim, T.Y., Han, S.K.: 10 Gbits all-optical composite logic gates with XOR, NOR, OR, and NAND functions using SOA-MZI structures. Electron. Lett. **42**, 303–307 (2006)
8. Martínez, J.M., Ramos, F., Martí, J.: 10 Gb/s reconfigurable optical logic gate using a single hybrid-integrated SOA-MZI. Fiber Integr. Opt. **27**, 15–20 (2008)
9. Singh, S., Lovkesh, : Ultrahigh-speed optical signal processing logic based on an SOA-MZI. IEEE J. Sel. Top. Quantum Electron. **18**, 970–975 (2012)
10. Sun, H., Wang, Q., Dong, H., Chen, Z., Dutta, N.K., Jaques, J., Piccirilli, A.B.: All-optical logic XOR gate at 80 Gb/s using SOA-MZI-DI. IEEE J. Quantum Electron. **42**, 747–751 (2006)
11. Kang, I., Rasras, M., Buhl, L., Dinu, M., Cabot, S., Cappuzzo, M., Gomez, L.T., Chen, Y.F., Patel, S.S., Dutta, N.K., Piccirilli, A.B., Jaques, J., Giles, C.R.: All-optical XOR and XNOR operations at 86.4 Gb/s using a pair of semiconductor optical amplifier Mach–Zehnder interferometers. Opt. Express **17**, 19062–19066 (2009)
12. Kotb, A., Zoiros, K.E.: Performance of all-optical XOR gate based on two-photon absorption in semiconductor optical amplifier-assisted Mach–Zehnder interferometer with effect of amplified spontaneous emission. Opt. Quantum Electron. **46**, 935–941 (2014)
13. Bogoni, A., Potì, L., Ghelfi, P., Scaffardi, M., Porzi, C., Ponzini, F., Meloni, G., Berrettini, G., Malacarne, A., Prati, G.: OTDM-based optical communications networks at 160 Gbit/s and beyond. Opt. Fiber Technol. **13**, 1–12 (2007)
14. Mulvad, H.C.H., Galili, M., Oxenløwe, L.K., Hu, H., Clausen, A.T., Lensen, J.B., Peucheret, C., Jeppesen, P.: Demonstration of 5.1 Tbit/s data capacity on a single-wavelength channel. Opt. Express **18**, 1438–1443 (2010)
15. Dúill, S.O., Marazzi, L., Parolari, P., Brenot, R., Koos, C., Freude, W., Leuthold, J.: Efficient modulation cancellation using reflective SOAs. Opt. Express **20**, 587–594 (2012)
16. Yu, X., Gibbon, T.B., Monroy, I.T.: Bidirectional radio-over-fiber system with phase-modulation downlink and RF oscillator-free uplink using a reflective SOA. IEEE Photon. Technol. Lett. **20**, 2180–2182 (2008)
17. Spiekman, L.H.: Active devices in passive optical networks. J. Lightwave Technol. **31**, 488–497 (2013)
18. Mukherjee, K.: A novel frequency encoded all-optical logic gates exploiting polarization insensitive four-wave mixing in semiconductor optical amplifier, filtering property of ADD/DROP multiplexer and non-linearity of reflective semiconductor amplifier. Optik **122**, 891–895 (2011)
19. Thollabandi, M., Jung, S.Y., Park, C.S.: All-optical wavelength conversion in GC-RSOA. In: ICTC 6082651, pp. 515–516 (2011)
20. Hu, Z., Sun, J.: All-optical logic NOT gate for Manchester encoded signal using a reflective semiconductor optical amplifier. Opt. Appl. **40**, 57–61 (2010)
21. Duill, S.O., Barry, L.P.: Improved reduced models for single-pass and reflective semiconductor optical amplifiers. Opt. Commun. **334**, 170–173 (2015)
22. Antonelli, C., Mecozzi, A.: Reduced model for the nonlinear response of reflective semiconductor optical amplifiers. IEEE Photon. Technol. Lett. **25**, 2243–2246 (2013)

23. Cassioli, D., Scotti, S., Mecozzi, A.: A time-domain computer simulator of the nonlinear response of semiconductor optical amplifiers. IEEE J. Quantum Electron. **36**, 1072–1080 (2000)
24. Antonelli, C., Mecozzi, A., Hu, Z., Santagiustina, M.: Analytic study of the modulation response of reflective semiconductor optical amplifiers. J. Lightwave Technol. **33**, 4367–4376 (2015)
25. Connelly, M.J.: Reflective semiconductor optical amplifier pulse propagation model. IEEE Photon. Technol. Lett. **24**, 95–97 (2012)
26. Sengupta, I., Barman, A.D.: Analysis of optical re-modulation by multistage modeling of RSOA. Optik **125**, 3393–3400 (2014)
27. Schares, L., Schubert, C., Schmidt, C., Weber, H.G., Occhi, L., Guekos, L.: Phase dynamics of semiconductor optical amplifiers at 10 to 40 GHz. IEEE J. Quantum Electron. **39**, 1394–1408 (2003)
28. Ueno, Y., Nakamura, S., Tajima, K.: Nonlinear phase shifts induced by semiconductor optical amplifiers with control pulses at repetition frequencies in the 40–160-GHz range for use in ultrahigh-speed all-optical signal processing. J. Opt. Soc. Am. B **19**, 2573–2589 (2002)
29. Giller, R., Manning, R.J., Talli, G., Webb, R.P., Adams, M.J.: Analysis of the dimensional dependence of semiconductor optical amplifier recovery speeds. Opt. Express **15**, 1773–1782 (2007)
30. Ma, S., Sun, H., Chen, Z., Dutta, N.K.: High speed all-optical PRBS generation based on quantum-dot semiconductor optical amplifiers. Opt. Express **17**, 18469–18477 (2009)
31. Rizou, Z.V., Zoiros, K.E., Hatziefremidis, A., Connelly, M.J.: Design analysis and performance optimization of a Lyot filter for semiconductor optical amplifier pattern effect suppression. J. Sel. Top. Quantum Electron. **19**, 1–9 (2013)
32. Kumar, Y., Shenoy, M.R.: Enhancement in the gain recovery of a semiconductor optical amplifier by device temperature control. Pramana J. Phys. **87**, 82 (2016)
33. Cho, K.Y., Hong, U.H., Choi, H., Chung, Y.C.: Maximum operable speed of WDM PON employing bandwidth-limited RSOAs. Opt. Commun. **312**, 159–162 (2014)
34. Agrawal, G.P., Olsson, N.A.: Self-phase modulation and spectral broadening of optical pulses in semiconductor laser amplifiers. IEEE J. Quantum Electron. **25**, 2297–2306 (1989)
35. Wei, J.L., Hamié, A., Gidding, R.P., Hugues-Salas, E., Zheng, X., Mansoor, S., Tang, J.M.: Adaptively modulated optical OFDM modems utilizing RSOAs as intensity modulators in IMDD SMF transmission systems. Opt. Express **18**, 8556–8573 (2010)
36. Zhou, E., Zhang, X., Huang, D.: Analysis on dynamic characteristics of semiconductor optical amplifiers with certain facet reflection based on detailed wideband model. Opt. Express **15**, 9096–9106 (2007)
37. Olsson, N.A.: Lightwave systems with optical amplifiers. J. Lightwave Technol. **7**, 1071–1082 (1989)
38. Wei, J.L., Yang, X.L., Giddings, R.P., Tang, J.M.: Colourless adaptively modulated optical OFDM transmitters using SOAs as intensity modulators. Opt. Express **17**, 9012–9027 (2009)
39. Siarkos, T., Zoiros, K.E., Nastou, D.: On the feasibility of full pattern-operated all-optical XOR gate with single semiconductor optical amplifier-based ultrafast nonlinear interferometer. Opt. Commun. **282**, 2729–2734 (2009)
40. MacWilliams, F.J., Sloane, N.J.A.: Pseudo-random sequences and arrays. Proc. IEEE **64**, 1715–1729 (1976)